

# Dynamics of biomembranes with active multiple-state inclusions

Hsuan-Yi Chen<sup>(1)(2)</sup> and Alexander S. Mikhailov<sup>(3)</sup>

<sup>(1)</sup>*Department of Physics and Institute of Biophysics,*

*National Central University,*

*Jhongli, 32001, Taiwan*

*and*

<sup>(2)</sup>*Institute of Physics,*

*Academia Sinica, Taipei, 11529, Taiwan*

*and*

<sup>(3)</sup>*Abteilung Physikalische Chemie,*

*Fritz-Haber-Institut der Max-Planck-Gesellschaft,*

*Faradayweg 4-6, 14195 Berlin, Germany*

(Dated: June 28, 2018)

## Abstract

Nonequilibrium dynamics of biomembranes with active inclusions is considered. The inclusions represent protein molecules which perform cyclic internal conformational motions driven by the energy brought with ATP ligands. As protein conformations cyclically change, this induces hydrodynamical flows and also directly affects the local curvature of a membrane. On the other hand, variations in the local curvature of the membrane modify the transitions rates between conformational states in a protein, leading to a feedback in the considered system. Moreover, active inclusions can move diffusively through the membrane so that surface concentration varies. The kinetic description of this system is constructed and the stability of the uniform stationary state is analytically investigated. We show that, as the rate of supply of chemical energy is increased above a certain threshold, this uniform state becomes unstable and stationary or traveling waves spontaneously develop in the system. Such waves are accompanied by periodic spatial variation of membrane curvature and inclusion density. For typical parameter values, their characteristic wavelengths are of the order of hundreds of nanometers. For traveling waves, the characteristic frequency is of the order of a thousand Hz or less.

PACS numbers: 87.16.Dg, 05.40.-a, 05.70.Np

## I. INTRODUCTION

Membranes play a fundamental role in various functions of living cells, providing spatial compartmentalization and being essential for signal transduction and inter- or intracellular transport [1]. While *in vivo* experiments with biomembranes are difficult because of their strong coupling to cytoskeleton and cytoplasm, investigations with synthetic membranes and vesicles formed by lipid bilayers can be performed [2]. Equilibrium morphology transitions in vesicles are well described by the elastic membrane theory [3]. However, it becomes increasingly clear that, under standard physiological conditions in a living cell, biomembranes are far from the state of thermal equilibrium.

Lipid bilayers that constitute a biomembrane are usually including a large number of protein molecules which may represent ion pumps, enzymes or other molecular machines. The common property of active protein inclusions is that they undergo cyclic conformational changes, with each next cycle initiated by binding of an energy-bringing ligand, typically an ATP molecule. Active conformational motions in the inclusions are coupled to membrane dynamics, thus bringing a membrane away from the state of thermodynamic equilibrium.

Theoretical investigations of biomembranes including active ion pumps have shown [4] that their fluctuational power spectra must be very different from that of the equilibrium membrane systems. It has been experimentally demonstrated that active inclusions renormalize bending rigidity [5, 6] and surface tension [7] of biological membranes. In several theoretical studies, it has been furthermore predicted [8, 9] that instabilities of membrane shapes may be induced by the nonequilibrium activity of the inclusions. Such instabilities could not however so far been observed in the experiments.

The original theoretical analysis of active membrane instabilities has been performed [8] in the framework of a general phenomenological approach where the details of operation of individual protein inclusions did not play a role. Effects of conformational transitions in active protein inclusions have been explicitly considered in the previous publication [9, 10] where the equations for membrane dynamics have been complemented by a kinetic equation for conformational transitions in molecular inclusions. Only inclusions with two different conformational states have been previously studied.

However, as we point it out now, models with two-state inclusions cannot describe generic properties of nonequilibrium membrane systems. Indeed, when only two discrete states are

present in active element and stochastic transitions between them take place, such transitions always satisfy the condition of detailed balance. Therefore, for such elements, there is no principal difference between the states of thermal equilibrium and nonequilibrium steady states, the latter being always describable as equilibrium states with some effective temperature.

In order to see true differences in the behavior of equilibrium and nonequilibrium membranes, inclusions with at least three internal conformational states must therefore be considered. For such inclusions, cyclic probabilities flows indicating the absence of the detailed balance are possible. The intensity of such flows provides direct characterization of the degree of deviation from thermal equilibrium.

Having this in mind, we construct here a complete kinetic description for the membranes with multiple-state inclusions, representing a generalization of the previous theories [4, 5, 9]. For the general case of the  $K$ -state inclusions, a detailed stability analysis is analytically performed. In addition to the long-wavelength static instability due to the negative effective surface tension, which has previously been known, two new instabilities are found. They are the Turing-type static instability with a finite spatial wavelength and the oscillatory wave-type instability with a finite wavelength. The characteristic wavelengths of both instabilities are of the order of hundreds of nanometers; the characteristic frequency of the patterns emerging as a result of the wave instability is up to a thousand Hz.

Below in Section II the theoretical model is formulated. First the expressions for the free energy of the system are given and then the dynamical evolution equations are constructed. In Section III, the slow-time limit of the model, valid when the time scales of intramolecular processes are much shorter than the time scales of the merging membrane patterns, is introduced and discussed. The stability analysis of the uniform stationary state is performed in Section IV. The results are finally discussed in Section V.

## II. THE MODEL

### A. Free energy and the equilibrium state

We consider a membrane composed of lipids and active inclusions with  $K$  internal states. In this study, we assume that all inclusions have the same orientation with respect to the

membrane. The situation where inclusions with both up and down orientations are present can be considered in a similar way. Before discussing the dynamics, we first consider the free energy of this system. At coarse-grained level, its free energy is given by the sum of the elastic energy of a lipid bilayer, the free energy associated with the inclusions, and the energy of coupling between the inclusions and the elastic membrane,

$$F = F_{mem} + F_{inc} + F_{coup}. \quad (1)$$

For a quasi-flat membrane, the elastic free energy of a lipid bilayer is

$$F_{mem} = \frac{1}{2} \int d^2r [\gamma(\nabla h)^2 + \kappa(\nabla^2 h)^2 + k_2(\nabla^3 h)^2], \quad (2)$$

where  $h$  is the height of the membrane relative to the reference plane,  $\mathbf{r} = x\hat{\mathbf{i}} + y\hat{\mathbf{j}}$  is the two-dimensional position vector in the reference plane, and  $\nabla = \partial_x\hat{\mathbf{i}} + \partial_y\hat{\mathbf{j}}$ . The coefficient  $\gamma$  characterizes surface tension of the membrane,  $\kappa$  specifies the bending rigidity of the membrane, and the coefficient  $k_2$  characterizes its rigidity with respect to the spatial variation of the curvature. Below, the last term is taken into account only for the short-wavelength instabilities, where it becomes essential and determines the instability wavelength. Since the system under consideration is a biomimetic membrane, we take the surface tension of typical cell membranes as the upper limit for the magnitude of  $\gamma$ , i.e.,  $\gamma \lesssim 5 \times 10^{-3} k_B T / \text{nm}^2$  [11]. The coefficient  $\kappa$  typically is  $\kappa \sim 10 k_B T$  [12], and  $k_2 \sim a^2 \kappa \sim 300 k_B T \cdot \text{nm}^2$  ( $a \sim 5 \text{nm}$  is the linear size of an inclusion).

The free energy associated with the inclusions is

$$F_{inc} = n_0 \int d^2r \left\{ k_B T \left[ \sum_{\alpha} \phi_{\alpha} \ln \phi_{\alpha} + (1 - \sum_{\alpha} \phi_{\alpha}) \ln(1 - \sum_{\alpha} \phi_{\alpha}) \right] + \sum_{\alpha} E_{\alpha} \phi_{\alpha} \right\}, \quad (3)$$

where  $0 \leq \phi_{\alpha} \leq 1$  is the dimensionless surface density of inclusions in the state  $\alpha$  ( $\alpha = 1, 2, 3, \dots, K$ ),  $E_{\alpha}$  is the energy of an inclusion in the state  $\alpha$ ,  $n_0 = 1/a^2$ . In this paper, we consider the case of the low inclusion density and neglect therefore possible direct lateral interactions between the inclusions.

The coupling between the inclusion density and the local membrane curvature is

$$F_{coup} = \int d^2r \kappa \sum_{\alpha} c_{\alpha} \phi_{\alpha} \nabla^2 h, \quad (4)$$

where  $c_{\alpha}$  are the coefficients specifying the strength of coupling between inclusions in different internal states  $\alpha$  and the local membrane curvature. When  $c_{\alpha} > 0$ , membrane regions rich

in the inclusions in the state  $\alpha$  tend to have  $\nabla^2 h < 0$ . The coefficient  $c_\alpha$  has dimension of inverse length,  $c_\alpha \sim \Delta\Sigma_\alpha/\Sigma_\alpha l_\alpha$  where  $\Sigma_\alpha$  is the average cross-sectional area,  $\Delta\Sigma_\alpha$  is the difference between the outer and inner leaflet surface area of a state- $\alpha$  inclusion, and  $l_\alpha$  is the thickness (in the  $z$  direction) of the inclusion (see Appendix for the explanations). Typically,  $c_\alpha$  is of the order of  $\leq 0.1\text{nm}^{-1}$ .

The equilibrium state of the system satisfies the conditions  $\delta F/\delta h = 0$  and  $\delta F/\delta\phi_\alpha = 0$ . This leads to the equations determining the equilibrium state,

$$\kappa\nabla^4 h - \gamma\nabla^2 h - k_2\nabla^6 h + \kappa \sum_{\alpha} c_\alpha \nabla^2 \phi_\alpha = 0, \quad (5)$$

and

$$\kappa c_\alpha \nabla^2 h + k_B T n_0 \left[ \ln \phi_\alpha - \ln \left( 1 - \sum_{\beta} \phi_\beta \right) \right] + n_0 E_\alpha = 0. \quad (6)$$

Eq. (6) gives us

$$\phi_\alpha = \left( 1 - \sum_{\beta} \phi_\beta \right) \exp \left[ - (E_\alpha + n_0^{-1} \kappa c_\alpha \nabla^2 h) / k_B T \right]. \quad (7)$$

Therefore the local total density of the inclusion in thermal equilibrium is simply

$$\phi_t = \sum_{\alpha} \phi_\alpha = \frac{\sum_{\alpha} \exp \left[ - (E_\alpha + n_0^{-1} \kappa c_\alpha \nabla^2 h) / k_B T \right]}{1 + \sum_{\alpha} \exp \left[ - (E_\alpha + n_0^{-1} \kappa c_\alpha \nabla^2 h) / k_B T \right]}. \quad (8)$$

Note that the total number of inclusions present in the membrane is  $N = n_0 \int d^2 r \phi_t$ . It depends on  $E_\alpha$ , implying that  $E_\alpha$  includes the contribution from the free energy difference between an  $\alpha$ -state inclusion in the membrane and an  $\alpha$ -state inclusion in the solvent.

Already the equilibrium state of the system may exhibit complex structural phases such as the undulated lamellar phase, the hexatic arrangement of inclusions, etc (see [13]). These phases are possible because of the strong coupling between the inclusion density and the local membrane curvature, and it has been argued that they are important for biological membranes [14]. Because we are primarily interested in the nonequilibrium behavior, we limit however our study below to the situations where the uniform flat state of the membrane is stable under equilibrium conditions.

## B. Evolution equations

If a membrane is impermeable, it can only move together with the solvent flow. A (partially) permeable membrane can be dragged through the solvent. Thus, the equation

for the temporal evolution of  $h(\mathbf{r}, t)$  is

$$\partial_t h = \mathbf{v} \cdot \hat{\mathbf{n}} - \lambda_p \left[ \frac{\delta F}{\delta h} + \sum_{\alpha, \beta} k_{\alpha\beta} n_0 P_{\alpha\beta}^m \phi_\beta \right], \quad (9)$$

where  $\mathbf{v}(\mathbf{r})$  is the local solvent flow and  $\hat{\mathbf{n}}(\mathbf{r})$  is the unit normal vector of the membrane surface. Because of the permeation, the solvent can “leak” from one side of the membrane to the other. If the force  $f$  is locally applied at a permeable membrane, it gets dragged through the solvent with the velocity  $v = \lambda_p f$ , where  $\lambda_p$  is the permeation constant. The local force  $f$  is given by the expression in the brackets in equation (9). In addition to the first contribution, directly coming from the free energy, it also includes the second term of purely kinetic origin. When an inclusion changes its internal conformational state, some force acting on the membrane is generated. Such average force corresponds to the second term inside the brackets. Here,  $k_{\alpha\beta}$  is the transition rate constant for an inclusion to go from state  $\beta$  to state  $\alpha$  and  $P_{\alpha\beta}^m$  is the momentum that an inclusion delivers to the membrane during a  $\beta \rightarrow \alpha$  conformational change. Typically  $P_{\alpha\beta}^m$  ranges from  $\text{pN} \cdot \mu\text{s}$  to  $\text{pN} \cdot \text{ms}$ . In our analysis, we shall neglect thermal noises acting on the membrane, which should be generally present in the membrane evolution equation.

The local density of inclusions in the state  $\alpha$  changes with time because of the lateral diffusion and the conformational transitions between the states, so that the evolution equations for the surface densities of inclusions in the state  $\alpha$  are

$$\partial_t \phi_\alpha = M_\alpha \nabla^2 \frac{\delta F}{\delta \phi_\alpha} + \sum_\beta [k_{\alpha\beta} \phi_\beta - k_{\beta\alpha} \phi_\alpha], \quad (10)$$

where  $M_\alpha$  is the mobility coefficient for the state- $\alpha$  inclusions.

Hydrodynamic flows in the solvent are described by the modified Stokes equation in the limit of low Reynolds number that takes into account the elastic stress due to the membrane and the forces resulting from the inclusion conformational changes. We have

$$\begin{aligned} 0 = & -\nabla p - \partial_z p \hat{\mathbf{z}} + \eta(\nabla^2 + \partial_z^2) \mathbf{v} - \delta(z-h) \frac{\delta F}{\delta h} \hat{\mathbf{n}} \\ & + \sum_{\alpha\beta} k_{\alpha\beta} n_0 P_{\alpha\beta}^m \phi_\beta \left[ (1 + z_{\alpha\beta}^{(u)} \nabla^2 h) \delta(z - z_{\alpha\beta}^{(u)} - h) - (1 - z_{\alpha\beta}^{(d)} \nabla^2 h) \delta(z + z_{\alpha\beta}^{(d)} - h) \right] \hat{\mathbf{n}}, \end{aligned} \quad (11)$$

where  $\eta$  is the viscosity of the solvent. In this equation,  $\delta F/\delta h$  corresponds to the pressure jump across the membrane due to the membrane elasticity. The last term comes from conformational changes of the inclusions.

Because the dynamics of an inclusion in the fluid is strongly overdamped, an inclusion exerts a zero net force on the solvent during its conformational transition from the state  $\beta$  to the state  $\alpha$ . The simplest description for the effect of an inclusion conformational change on the solvent flow is therefore provided by a model of a force dipole.  $z_{\alpha\beta}^{(u)}$  and  $z_{\alpha\beta}^{(d)}$  in Eq. (11) are characteristic lengths (both on the order of nm) for the force distribution during a conformational change of an inclusion from the state  $\beta$  to the state  $\alpha$ . As has been previously pointed out in Ref. [15], but neglected in Refs. [6] and [9], because force centers of the inclusions lie in the surfaces parallel to the membrane (see Fig. 1) the local density of the force centers in the plane  $h + z_{\alpha\beta}^{(u)}$  is  $(1 + z_{\alpha\beta}^{(u)}\nabla^2 h)\delta(z - z_{\alpha\beta}^{(u)} - h)$  and the local density of the force centers in the plane  $h - z_{\alpha\beta}^{(d)}$  is  $(1 - z_{\alpha\beta}^{(d)}\nabla^2 h)\delta(z + z_{\alpha\beta}^{(d)} - h)$ .

In addition, because the solvent is incompressible we have

$$\nabla \cdot \mathbf{v} + \partial_z v_z = 0. \quad (12)$$

### C. Microscopic reversibility and detailed balance

Microscopic reversibility imposes several constraints on  $k_{\alpha\beta}$ ,  $P_{\alpha\beta}^m$ ,  $P_{\alpha\beta}$ ,  $z_{\alpha\beta}^{(u)}$ , and  $z_{\alpha\beta}^{(d)}$ . The local membrane curvature affects the energy landscape of the conformational states of an inclusion, thus in general the transition rates  $k_{\alpha\beta}$  should depend on the local membrane curvature. To the order of  $\nabla^2 h$  we have

$$k_{\alpha\beta} = \Omega_{\alpha\beta}^{(0)} k_{\alpha\beta}^{(0)} \left(1 + \Omega_{\alpha\beta}^{(1)} l_{\alpha\beta} \nabla^2 h\right). \quad (13)$$

Here, the parameters  $k_{\alpha\beta}^{(0)}$  and  $l_{\alpha\beta}$  correspond to passive inclusions, in the absence of external energy supply;  $k_{\alpha\beta}^{(0)}$  is the equilibrium transition rate and  $l_{\alpha\beta}$  represents the characteristic length associated with the curvature dependence of  $k_{\alpha\beta}^{(0)}$ . The parameters  $\Omega_{\alpha\beta}^{(0)}$  and  $\Omega_{\alpha\beta}^{(1)}$  are introduced to describe changes in these properties when inclusions become active, i.e. when the energy is supplied to the inclusions. Thus, for passive inclusions  $\Omega_{\alpha\beta}^{(0)} = \Omega_{\alpha\beta}^{(1)} = 1$  and the transition rates take the equilibrium form  $k_{\alpha\beta} = k_{\alpha\beta}^e = k_{\alpha\beta}^{(0)}(1 + l_{\alpha\beta}\nabla^2 h)$ .

The detailed balance condition implies (to the order  $h$ ) the following relationship between the equilibrium transition rates  $k_{\alpha\beta}^e$  and  $k_{\beta\alpha}^e$ ,

$$\frac{k_{\alpha\beta}^e}{k_{\beta\alpha}^e} = \frac{e^{-(E_\alpha + n_0^{-1}\kappa c_\alpha \nabla^2 h)/k_B T}}{e^{-(E_\beta + n_0^{-1}\kappa c_\beta \nabla^2 h)/k_B T}} = e^{-(E_\alpha - E_\beta)/k_B T} \left(1 - \frac{\kappa(c_\alpha - c_\beta)}{n_0 k_B T} \nabla^2 h\right). \quad (14)$$



The second expression is valid as long as  $\kappa(c_\alpha - c_\beta)\nabla^2 h/n_0 k_B T = [\kappa(c_\alpha - c_\beta)/n_0 k_B T]/R \ll 1$ , where  $R = |\nabla^2 h|^{-1}$  is the radius of the local membrane curvature. The above condition yields

$$\frac{k_{\alpha\beta}^{(0)}}{k_{\beta\alpha}^{(0)}} = e^{-(E_\alpha - E_\beta)/k_B T}, \quad (15)$$

and

$$l_{\alpha\beta} - l_{\beta\alpha} = -\frac{\kappa(c_\alpha - c_\beta)}{n_0 k_B T}. \quad (16)$$

When the system is passive, there can be no active permeation. Therefore, we have

$$\sum_{\alpha\beta} k_{\alpha\beta}^e P_{\alpha\beta}^m \phi_\beta = 0. \quad (17)$$

The requirement of the detailed balance  $k_{\alpha\beta}^e \phi_\beta^e = k_{\beta\alpha}^e \phi_\alpha^e$  yields

$$P_{\alpha\beta}^m = -P_{\beta\alpha}^m. \quad (18)$$

This relationship is a direct consequence of the microscopic reversibility of an  $\alpha \rightarrow \beta$  transition: the momentum transfer from an inclusion to the membrane during an  $\alpha \rightarrow \beta$  transition has the same magnitude but opposite direction as the momentum transfer from an inclusion to the membrane during a  $\beta \rightarrow \alpha$  transition.

Two other conditions that must be satisfied for passive systems are

$$\left\{ \begin{array}{l} \sum_{\alpha\beta} k_{\alpha\beta}^e P_{\alpha\beta} (z_{\alpha\beta}^{(u)} + z_{\alpha\beta}^{(d)}) \phi_\beta = 0, \\ \sum_{\alpha\beta} k_{\alpha\beta}^e P_{\alpha\beta} (z_{\alpha\beta}^{(u)2} - z_{\alpha\beta}^{(d)2}) \phi_\beta = 0. \end{array} \right.$$

Again, because of the detailed balance, these two conditions lead to

$$P_{\alpha\beta} = -P_{\beta\alpha}, \quad (19)$$

and

$$z_{\alpha\beta}^{(u)} = z_{\beta\alpha}^{(u)}, \quad z_{\alpha\beta}^{(d)} = z_{\beta\alpha}^{(d)}. \quad (20)$$

These conditions are also direct consequences of microscopic reversibility.

#### D. Final evolution equations

By using equations (11) and (12) and applying the Fourier transformation in the coordinate space, the flow velocity  $\mathbf{v}$  can be expressed in terms of the height variation  $h$ . Substituting the resulting expressions into (9) and (10), final evolution equations for the membrane height and the inclusion density in different conformation states are obtained. They have the form

$$\begin{aligned} \partial_t h(\mathbf{q}, t) = & -\lambda_p \left[ \frac{\delta F}{\delta h} + \sum_{\alpha\beta} k_{\alpha\beta} n_0 P_{\alpha\beta}^m \phi_\beta \right] (\mathbf{q}, t) \\ & - \frac{1}{4\eta q} \left[ \frac{\delta F}{\delta h} + \sum_{\alpha\beta} k_{\alpha\beta} n_0 P_{\alpha\beta} \phi_\beta (z_{\alpha\beta}^{(u)} + z_{\alpha\beta}^{(d)}) q^2 h + \sum_{\alpha\beta} k_{\alpha\beta} n_0 P_{\alpha\beta} \frac{z_{\alpha\beta}^{(u)2} - z_{\alpha\beta}^{(d)2}}{2} q^2 \phi_\beta \right] (\mathbf{q}, t), \end{aligned} \quad (21)$$

and

$$\partial_t \phi_\alpha(\mathbf{q}, t) = -M_\alpha q^2 \frac{\delta F}{\delta \phi_\alpha}(\mathbf{q}, t) + \sum_{\beta} (k_{\alpha\beta} \phi_\beta - k_{\beta\alpha} \phi_\alpha) (\mathbf{q}, t). \quad (22)$$

Here  $h(\mathbf{q}, t)$  and  $\phi_\alpha(\mathbf{q}, t)$  are the coefficients of the Fourier expansion of the local height  $h(\mathbf{r}, t)$  and the local densities  $\phi_\alpha(\mathbf{r}, t)$  over the plane waves  $\exp(i\mathbf{q} \cdot \mathbf{r})$ .

The contributions to the membrane dynamics given by Eq. (21) come (i) from the direct momentum transfer from the inclusions to the lipid bilayer, described by  $k_{\alpha\beta} n_0 P_{\alpha\beta}^m \phi_\beta$ ; (ii) from the action of the active force dipoles due to the coupling between the local membrane curvature and the force density distribution, described by  $k_{\alpha\beta} n_0 P_{\alpha\beta} \phi_\beta (z_{\alpha\beta}^{(u)} + z_{\alpha\beta}^{(d)}) q^2 h$ ; and (iii) from the action of the active force quadrupoles due to the up-down asymmetry of the shape of the inclusions, described by  $k_{\alpha\beta} n_0 P_{\alpha\beta} (z_{\alpha\beta}^{(u)2} - z_{\alpha\beta}^{(d)2}) q^2 \phi_\beta / 2$ .

Evolution equations (21) and (22) provide the final concise description of the membrane dynamics coupled to the kinetic transitions in active multiple-state inclusions diffusing within the membrane. The physical meanings and typical magnitudes of the parameters entering into these equations and the respective expressions for the free energy are summarized in Table I.

Equations (21) and (22) represent the generalization of the equations previously obtained in the theories [8, 15] that neglected conformational changes inside the inclusions, where active momentum transfer from the inclusions to the membrane [8] and active force dipoles and active force quadrupoles [15] were both taken into account.

### III. THE LIMIT OF SLOW MEMBRANE DYNAMICS

Membrane motions with long wavelengths are slow. The characteristic time scales of such motions are much larger than the characteristic times corresponding to the the kinetics of internal transitions inside the inclusions. In this situation, which we consider further in our study, the steady nonequilibrium distribution over the internal states of active inclusions should adiabatically following the changes in the local membrane shape.

For example, let us consider biomembranes with active ion pumps, such as bacteriorhodopsin (BR) and  $\text{Ca}^{2+}$ -ATPase, which have used in the experiments [5, 6, 7]. The typical timescale for conformational transitions inside the cycle in these ion pumps is of the order of several milliseconds. The lateral diffusion constant for an an ion pump inside a membrane is on the order of  $1\mu\text{m}^2/s$ . Therefore, within a single active conformational cycle such an inclusion would move over the distance of about several tens of nanometers inside the membrane. Hence, if the membrane shape varies on a scale of several hundreds of nanometers or longer, the adiabatical approximation for the inclusion kinetics shall be applicable. In the steady state, local inclusion densities satisfy the equations

$$\sum_{\beta} (k_{\alpha\beta}\phi_{\beta} - k_{\beta\alpha}\phi_{\alpha}) = 0 \quad \text{for all } \alpha. \quad (23)$$

In this paper, inclusions with cyclic transitions are considered (Fig.2), so that  $k_{\alpha\beta} = 0$  for  $\beta - \alpha \neq \pm 1$ . Therefore, Eqs. (23) give us

$$k_{21}\phi_1 - k_{12}\phi_2 = k_{32}\phi_2 - k_{23}\phi_3 = k_{43}\phi_3 - k_{34}\phi_4 = \dots \equiv K_s(k_{\alpha\beta})\phi_t. \quad (24)$$

Thus, conformational transitions are characterized by a steady conformational current  $K_s\phi_t$ . When  $K_s > 0$  the conformational current is along  $1 \rightarrow 2 \rightarrow 3 \rightarrow \dots \rightarrow K \rightarrow 1$ . The presence of such a flow (if  $K_s$  is not vanishing) indicates the absence of detailed balance and the deviation from the state of thermal equilibrium for the inclusions.

Slow dynamics of the system is described by two variables: membrane height  $h$  and the total density of inclusions  $\phi_t = \sum_{\alpha} \phi_{\alpha}$ . From Eq. (22), we obtain

$$\partial_t \phi_t(\mathbf{r}, t) = \sum_{\alpha} M_{\alpha} \nabla^2 \left( k_B T n_0 \ln \frac{\phi_{\alpha}}{1 - \phi_t} + \kappa c_{\alpha} \nabla^2 h \right). \quad (25)$$

Here  $\phi_{\alpha}$  is a function of  $\phi_t$  and  $K_s$ , we will discuss this function later after deriving the linearized equations. To find the equation for  $h$ , terms related to active forces are simplified

by introducing the active momentum transfer, the active force dipole and the active force quadrupole associated with an inclusion. From Eqs. (18), (19), and (24), we obtain

$$\sum_{\alpha\beta} k_{\alpha\beta} P_{\alpha\beta}^m \phi_\beta = (P_{21}^m + P_{32}^m + \dots + P_{K-1}^m + P_{1K}^m)(k_{21}\phi_1 - k_{12}\phi_2) \equiv P_A^m K_s(k_{\alpha\beta})\phi_t, \quad (26)$$

$$\begin{aligned} & \sum_{\alpha\beta} k_{\alpha\beta} P_{\alpha\beta}(z_{\alpha\beta}^{(u)} + z_{\alpha\beta}^{(d)})\phi_\beta \\ &= \left[ P_{21}(z_{21}^{(u)} + z_{21}^{(d)}) + P_{32}(z_{32}^{(u)} + z_{32}^{(d)}) + \dots + P_{1K}(z_{1K}^{(u)} + z_{1K}^{(d)}) \right] (k_{21}\phi_1 - k_{12}\phi_2) \\ &\equiv p_A K_s \phi_t. \end{aligned} \quad (27)$$

and

$$\begin{aligned} & \sum_{\alpha\beta} k_{\alpha\beta} P_{\alpha\beta} \frac{z_{\alpha\beta}^{(u)^2} - z_{\alpha\beta}^{(d)^2}}{2} \phi_\beta \\ &= \left( P_{21} \frac{z_{21}^{(u)^2} - z_{21}^{(d)^2}}{2} + P_{32} \frac{z_{32}^{(u)^2} - z_{32}^{(d)^2}}{2} + \dots + P_{1K} \frac{z_{1K}^{(u)^2} - z_{1K}^{(d)^2}}{2} \right) (k_{21}\phi_1 - k_{12}\phi_2) \\ &\equiv Q_A K_s \phi_t. \end{aligned} \quad (28)$$

Here, we have defined the active momentum transfer from an inclusion to the membrane during one cycle  $P_A^m = P_{21}^m + P_{32}^m + \dots + P_{1K}^m$ , the net active force dipole of an inclusion during one cycle  $p_A = P_{21}(z_{21}^{(u)} + z_{21}^{(d)}) + P_{32}(z_{32}^{(u)} + z_{32}^{(d)}) + \dots + P_{1K}(z_{1K}^{(u)} + z_{1K}^{(d)})$ , and the net active force quadrupole of an inclusion during one cycle  $Q_A = P_{21}(z_{21}^{(u)^2} - z_{21}^{(d)^2})/2 + P_{32}(z_{32}^{(u)^2} - z_{32}^{(d)^2})/2 + \dots + P_{1K}(z_{1K}^{(u)^2} - z_{1K}^{(d)^2})/2$ . Note, that the respective terms are non-vanishing and thus contribute to the membrane dynamics only when the detailed balance is violated and the cyclic conformational current  $K_s \phi_t$  is present. The equation of motion for  $h(\mathbf{q}, t)$  can be obtained by substituting Eq. (26), (27), and Eq. (28) into Eq. (21), yielding

$$\begin{aligned} \partial_t h(\mathbf{q}, t) &= -\lambda_p \left[ \frac{\delta F}{\delta h} + n_0 P_A^m K_s \phi_t \right] (\mathbf{q}, t) \\ &\quad - \frac{1}{4\eta q} \left[ \frac{\delta F}{\delta h} + n_0 p_A K_s \phi_t h q^2 + n_0 Q_A K_s \phi_t q^2 \right] (\mathbf{q}, t). \end{aligned} \quad (29)$$

Eq. (29) indicates that the membrane acquires a nonzero velocity due to active permeation, as one can see from  $\partial_t h = -\lambda_p n_0 P_A^m K_s \phi_t$  at  $q = 0$ . For a permeable membrane this drift provides clear manifestation of non-equilibrium processes in the system under consideration.

#### IV. NONEQUILIBRIUM INSTABILITIES

To analyze possible instabilities of the flat membrane, we should linearize the equations of motion by expanding  $h(\mathbf{r}, t)$  and  $\phi_t(\mathbf{r}, t)$  around their uniform solutions  $h_0(t)$  and  $\phi_{t0}$ ,

$$\begin{aligned} h(\mathbf{r}, t) &= h_0(t) + \delta h(\mathbf{r}, t), \\ \phi_t(\mathbf{r}, t) &= \phi_{t0} + \delta\phi_t(\mathbf{r}, t). \end{aligned} \quad (30)$$

Note that  $\delta h(\mathbf{q}, t) = h(\mathbf{q}, t)$  and  $\delta\phi_t(\mathbf{q}, t) = \phi_t(\mathbf{q}, t)$  for  $q \neq 0$ .

First, we consider the linear elasticity of the system. One can express  $\delta F/\delta h$  as

$$\frac{\delta F}{\delta h(\mathbf{r})} = (\kappa\nabla^4 - \gamma\nabla^2 - k_2\nabla^6)h + \sum_{\alpha} \kappa c_{\alpha} \nabla^2 \left( \frac{\phi_{\alpha}}{\phi_t} \phi_t \right).$$

At small  $\nabla^2 h$ , we can further express  $\phi_{\alpha}/\phi_t$  as

$$\frac{\phi_{\alpha}}{\phi_t} = \psi_{\alpha} (1 + l_{\psi\alpha} \nabla^2 h + \dots), \quad (31)$$

where  $\psi_{\alpha}$  is dimensionless and  $l_{\psi\alpha}$  is a length that characterizes the curvature dependence of  $\phi_{\alpha}/\phi_t$ . Because all coordinate dependence of  $\phi_{\alpha}/\phi_t$  comes from the local curvature dependence of the transition rates, both  $\psi_{\alpha}$  and  $l_{\psi\alpha}$  are independent of  $\mathbf{r}$ , but they depend on  $\Omega_{\alpha\beta}^{(0)}$  and  $\Omega_{\alpha\beta}^{(1)}$ , i.e., on the strength of the external energy drive. From Eq. (31),  $\nabla^2(\phi_t\phi_{\alpha}/\phi_t) = \psi_{\alpha}\nabla^2\phi_t + \psi_{\alpha}l_{\psi\alpha}\phi_{t0}\nabla^4h + \dots$ . As a result

$$\begin{aligned} \frac{\delta F}{\delta h(\mathbf{r})} &= \kappa(1 + \sum_{\alpha} c_{\alpha}\psi_{\alpha}l_{\psi\alpha}\phi_{t0})\nabla^4h - \gamma\nabla^2h - k_2\nabla^6h + \sum_{\alpha} \kappa c_{\alpha}\psi_{\alpha}\nabla^2\phi_t \\ &= \kappa_{eff}\nabla^4h - \gamma\nabla^2h - k_2\nabla^6h + \kappa_{eff}c_{eff}^h\nabla^2\phi_t. \end{aligned} \quad (32)$$

Here we have introduced the effective membrane bending rigidity  $\kappa_{eff} = \kappa(1 + \sum_{\alpha} c_{\alpha}\psi_{\alpha}l_{\psi\alpha}\phi_{t0})$  and the effective inclusion-membrane elastic coupling constant  $c_{eff}^h = \sum_{\alpha} c_{\alpha}\psi_{\alpha}\kappa/\kappa_{eff}$ . Note that, besides  $c_{\alpha}$ ,  $\kappa_{eff}$  and  $c_{eff}^h$  also depend on  $\Omega_{\alpha\beta}^{(0)}$  and  $\Omega_{\alpha\beta}^{(1)}$  through  $\psi_{\alpha}$  and  $l_{\psi\alpha}$ . These effective elastic moduli are different from their equilibrium values because the relative inclusion population  $\phi_{\alpha}/\phi_t$  is different from the equilibrium distribution.

Next we consider the equation for  $\delta\phi_t$ . From Eq. (31),

$$\begin{aligned} \nabla^2 \left( \ln \frac{\phi_{\alpha}}{1 - \phi_t} \right) &= \nabla^2 \left( \ln \frac{\phi_{\alpha}}{\phi_t} + \ln \frac{\phi_t}{1 - \phi_t} \right) \\ &= l_{\psi\alpha} \nabla^4 h + \left( \frac{1}{\phi_{t0}} + \frac{1}{1 - \phi_{t0}} \right) \nabla^2 \delta\phi_t \end{aligned}$$

Substituting the above expression into Eq. (25), one finds

$$\partial_t \delta \phi_t = \sum_{\alpha} M_{\alpha} \left\{ n_0 k_B T \left[ l_{\psi\alpha} \nabla^4 h + \left( \frac{1}{\phi_{t0}} + \frac{1}{1 - \phi_{t0}} \right) \nabla^2 \delta \phi_t \right] + \kappa c_{\alpha} \nabla^4 h \right\}.$$

It is convenient to introduce the effective mobility  $M_{eff} \equiv \sum_{\alpha} M_{\alpha}$ , the effective susceptibility of the inclusions  $\chi_{eff} \equiv n_0 k_B T [1/\phi_{t0} + 1/(1 - \phi_{t0})]$  and the effective inclusion-membrane elastic coupling constant  $c_{eff}^{\phi}$  associated with inclusion diffusion,  $M_{eff} \kappa_{eff} c_{eff}^{\phi} \equiv \sum_{\alpha} M_{\alpha} (\kappa c_{\alpha} + n_0 k_B T l_{\psi\alpha})$ . Similar to  $\kappa_{eff}$  and  $c_{eff}^h$ ,  $c_{eff}^{\phi}$  depends on  $\Omega_{\alpha\beta}^{(0)}$  and  $\Omega_{\alpha\beta}^{(1)}$ . Now the equation for  $\partial_t \phi_t(\mathbf{q}, t)$  can be written as

$$\partial_t \phi_t(\mathbf{q}, t) = -M_{eff} \left( \chi_{eff} q^2 \phi_t(\mathbf{q}, t) - \kappa_{eff} c_{eff}^{\phi} q^4 h(\mathbf{q}, t) \right). \quad (33)$$

To obtain the linearized equation for  $\partial h(\mathbf{q}, t)/\partial t$ , we expand the conformational current to the order of  $h$  as  $K_s(k_{\alpha\beta}) = K_0(1 + l_K \nabla^2 h + \dots)$  and obtain

$$K_s(k_{\alpha\beta}) \phi_t = K_0 \phi_{t0} + K_0 \delta \phi_t + K_0 l_K \phi_{t0} \nabla^2 h, \quad (34)$$

where  $K_0$  and  $l_K$  are both independent of  $\mathbf{r}$ , but they depend on  $\Omega_{\alpha\beta}^{(0)}$  and  $\Omega_{\alpha\beta}^{(1)}$ . Substituting Eq. (32) and (34) into Eq. (29), the linearized equation of motion for  $h(\mathbf{q}, t)$  in the momentum space is found,

$$\begin{aligned} \partial_t h(\mathbf{q}, t) = & -\lambda_p \left[ (\gamma_a^p q^2 + \kappa_{eff} q^4 + k_2 q^6) h(\mathbf{q}, t) - (\kappa_{eff} c_{eff}^h q^2 - n_0 P_A^m K_0) \phi_t(\mathbf{q}, t) \right] \\ & - \frac{1}{4\eta q} \left[ (\gamma_a q^2 + \kappa_a q^4 + k_2 q^6) h(\mathbf{q}, t) - \kappa_{eff} c_a q^2 \phi_t(\mathbf{q}, t) \right]. \end{aligned} \quad (35)$$

In this equation, following notations have been introduced:

$$\gamma_a^p = \gamma - n_0 P_A^m K_0 l_K \phi_{t0} \quad (36)$$

is the surface tension renormalized by active forces that inclusions act on the membrane,

$$\gamma_a = \gamma + n_0 p_A K_0 \phi_{t0} \quad (37)$$

is the surface tension renormalized by active force dipoles,

$$\kappa_a = \kappa_{eff} - n_0 Q_A K_0 l_K \phi_{t0} \quad (38)$$

is the bending rigidity renormalized by curvature-induced active quadrupoles, and

$$\kappa_{eff} c_a = \kappa_{eff} c_{eff}^h - n_0 Q_A K_0 \quad (39)$$

defines the renormalized inclusion-curvature coupling due to curvature-independent active force quadrupoles.

Since experiments are usually carried out for the membranes with negligible permeability [5, 6, 7], we consider below only instabilities of impermeable membranes with  $\lambda_p = 0$ .

It is convenient to write the derived the equations in the matrix form

$$\partial_t \begin{pmatrix} h(\mathbf{q}, t) \\ \phi_t(\mathbf{q}, t) \end{pmatrix} = \begin{pmatrix} M_{hh}(q) & M_{h\phi}(q) \\ M_{\phi h}(q) & M_{\phi\phi}(q) \end{pmatrix} \begin{pmatrix} h(\mathbf{q}, t) \\ \phi_t(\mathbf{q}, t) \end{pmatrix}, \quad (40)$$

where

$$\begin{aligned} M_{hh}(q) &= -\frac{q}{4\eta}(\gamma_a + \kappa_a q^2 + k_2 q^4), \\ M_{h\phi}(q) &= \frac{q}{4\eta} \kappa_{eff} c_a, \\ M_{\phi h}(q) &= M_{eff} \kappa_{eff} c_{eff}^\phi q^4, \\ M_{\phi\phi}(q) &= -M_{eff} \chi_{eff} q^2. \end{aligned} \quad (41)$$

The definitions and physical meanings of the parameters in Eq. (40) (41) are summarized in Table II.

To analyze the linear stability of the system, we seek solutions of Eq. (40) of the form  $h(\mathbf{q}, t), \phi_t(\mathbf{q}, t) \sim e^{\lambda t}$ . The characteristic equation for  $\lambda$  is

$$\lambda^2 - (M_{hh} + M_{\phi\phi})\lambda + (M_{hh}M_{\phi\phi} - M_{\phi h}M_{h\phi}) = 0. \quad (42)$$

Let the two solutions of the above equation be  $\lambda_1(\mathbf{q}), \lambda_2(\mathbf{q})$ , then

$$\begin{aligned} \lambda_1 + \lambda_2 &= M_{hh} + M_{\phi\phi} = -\frac{1}{4\eta} (\gamma_a q + 4\eta M_{eff} \chi_{eff} q^2 + \kappa_a q^3 + k_2 q^5), \\ \lambda_1 \lambda_2 &= M_{hh} M_{\phi\phi} - M_{\phi h} M_{h\phi} = \frac{M_{eff} \chi_{eff}}{4\eta} (\gamma_a q^3 + \tilde{\kappa}_a q^5 + k_2 q^7), \end{aligned} \quad (43)$$

where

$$\tilde{\kappa}_a = \kappa_a - \frac{\kappa_{eff}^2 c_a c_{eff}^\phi}{\chi_{eff}}. \quad (44)$$

The following instabilities can occur in this system:

- (i) A long-wavelength instability at  $q = 0$  when one of the  $\lambda$  becomes zero at  $q = 0$  and both  $\lambda_1, \lambda_2$  are negative for any nonzero  $q$ .
- (ii) An oscillatory wave instability (a Hopf bifurcation with a finite wavenumber)

at  $q = q_h$ , when  $\lambda_1 + \lambda_2 = M_{hh}(q) + M_{\phi\phi}(q) < 0$  for all  $q$  except  $q = q_h$  and  $\lambda_1\lambda_2 = M_{hh}(q)M_{\phi\phi}(q) - M_{h\phi}(q)M_{\phi h}(q) > 0$  for all  $q$ . The frequency of the wave at the onset of the instability is  $\omega/2\pi = \sqrt{\lambda_1(q_h)\lambda_2(q_h)}/2\pi$ .

(iii) A static Turing-type instability when  $\lambda_1 + \lambda_2 < 0$  for all  $q$  and  $\lambda_1\lambda_2 > 0$  for all  $q$  except  $q = q_s$ .

The typical magnitudes of the parameters that are important for stability analysis are summarized in Table III. Figure 3 shows the phase diagrams for systems with typical parameters. Varying the parameters does not change the qualitative features of the phase diagrams. The ordinates in Fig. 3 represent the strength of curvature-dependent pumping, and the abscissas represent the strength of curvature-independent pumping. The state of thermal equilibrium corresponds to the origin of coordinates; as the system is driven out of equilibrium, the state of the system moves along a straight line with the slope  $l_K/a$ . Generally, coefficients  $\kappa_{eff}$ ,  $c_{eff}^\phi$ , and  $c_{eff}^h$  also vary as the system is being moved away of equilibrium; for simplicity we take however constant values  $\kappa_{eff} = 5k_B T$ , and  $c_{eff}^\phi = c_{eff}^h = 0.1\text{nm}^{-1}$  when the phase boundaries below in Fig. 3 are determined.

### A. The long-wavelength static instability

According to Eq. (43), this instability occurs when  $\gamma_a = \gamma + n_0 p_A K_0 \phi_{t0} < 0$ , i.e. when the effective surface tension becomes negative. As shown in Fig. 3, for systems with  $p_A < 0$  this instability is possible at sufficiently large  $K_0$ . Using as typical values  $|p_A| \sim \text{nm} \cdot \text{pN} \cdot \mu\text{s}$  to  $\text{nm} \cdot \text{pN} \cdot \text{ms}$ ,  $K_0 \lesssim \text{ms}^{-1}$  and  $n_0 = a^{-2} \sim 1/25\text{nm}^2$ , we find that to get  $\gamma_a < 0$  for relatively low inclusion density, such as  $\phi_{t0} \lesssim 10^{-1}$ , a vesicle with the bare surface tension  $\gamma \lesssim 10^{-3}k_B T/\text{nm}^2$  is needed. In the experiments [7], the measured surface tension of a vesicle with passive BRs was  $\gamma \sim 10^{-4}k_B T/\text{nm}^2$ . Thus, it should be possible to observe this long-wavelength instability in the experiments.

### B. The finite-wavelength instabilities

Besides the long-wavelength instability corresponding to negative  $\gamma_a$ , there are also instabilities when  $\kappa_a$  or  $\tilde{\kappa}_a$  become negative. If  $\gamma_a$  is positive, these instabilities correspond



to the growth of modes with finite wavelengths, because long-wavelength fluctuations are suppressed by the membrane tension.

(i) When

$$\tilde{\kappa}_a = -2\sqrt{\gamma_a k_2}, \quad (45)$$

the static *Turing-type instability* takes place. Its characteristic wavenumber is

$$q_s = (\gamma_a/k_2)^{1/4}. \quad (46)$$

As follows from Eqs. (37), (38) and (44), Eq. (45) is equivalent to

$$n_0 Q_A K_0 \left( l_K \phi_{t0} - \frac{\kappa_{eff} c_{eff}^\phi}{\chi_{eff}} \right) - 2\sqrt{(\gamma + n_0 p_A K_0 \phi_{t0}) k_2} = \kappa_{eff} - \frac{\kappa_{eff}^2 c_{eff}^\phi c_{eff}^h}{\chi_{eff}}. \quad (47)$$

As seen in Fig. 4, two conditions are essential for the occurrence of this instability. The first is that the difference  $\kappa_{eff} - \kappa_{eff}^2 c_{eff}^\phi c_{eff}^h / \chi_{eff}$  should be small, implying that the curved membrane regions are strongly attracting the inclusions. The second property is that the combination  $n_0 Q_A K_0 (l_K \phi_{t0} - \kappa_{eff} c_{eff}^\phi / \chi_{eff})$  should be large and positive, implying strong curvature-induced active force quadrupoles. In the phase diagram in Fig. 3, the Turing-type instability is located where  $K_0 l_K$  is large.

The characteristic wavelength at the onset of the Turing-type instability can be estimated. Taking  $\gamma_a \sim \gamma \lesssim 5 \times 10^{-3} k_B T / \text{nm}^2$ ,  $k_2 \sim 300 k_B T \cdot \text{nm}^2$ , we find that this finite-wavelength instability has a characteristic wavelength of  $2\pi/q_s = 2\pi/(\gamma_a/k_2)^{1/4} \gtrsim 10\text{nm} - 10^2\text{nm}$ . Numerically computed wavelengths for this instability are shown in Fig. 5. Note also that, according to Fig. 3 and Fig. 5, for  $p_A < 0$  only the membranes with inclusions that have large  $l_0$  (i.e., the activity of these inclusions is induced by membrane curvature) may exhibit the Turing-type instability, otherwise long-wavelength instability is taking place.

(ii) When  $\kappa_a = \kappa_a^c$ , the oscillatory *wave instability* with the characteristic wavevector  $q_h$  takes place. The values of  $\kappa_a$  and  $q_h$  are given by the solutions of two equations,

$$q_h = \sqrt{\frac{-\kappa_a^c}{6k_2} + \sqrt{\left(\frac{-\kappa_a^c}{6k_2}\right)^2 + \frac{\gamma_a}{3k_2}}}, \quad (48)$$

and

$$2q_h^3 + \frac{\kappa_a^c}{k_2} q_h + \frac{2\eta M_{eff} \chi_{eff}}{k_2} = 0. \quad (49)$$

Because  $q_h > 0$ , Eq. (48) requires  $\kappa_a^c$  to be negative. Generally, the above equations for  $\kappa_a^c$  and  $q_h$  have to be solved numerically. Fig. 3 shows that this instability may occur only when  $p_A$ ,  $Q_A$ , and  $c_{eff}^h, c_{eff}^\phi$  all have the same sign, and the curvature-induced pumping is not too strong (i.e.,  $l_K$  is not very large). This condition suggests the following picture for the mechanism of wave instability. As shown in Fig. 6, first, inclusions are attracted to the regions with their preferred membrane curvature; but the active forces from the inclusions in these regions produce curvature that the inclusion dislike (thus  $l_K$  cannot be large). As a result, the inclusions move back and forth, chasing regions with preferred membrane curvature. This leads to an oscillatory instability with the characteristic wavelength which is large as compared to the molecular scale.

The characteristic wavelength at the onset of wave instability is about  $2\pi/q_h \sim 100\text{nm}$ . Substituting  $q_h$  to  $\omega_h = \sqrt{\lambda_1(q_h)\lambda_2(q_h)}$ , the characteristic time at the onset of wave instability is estimated to be of the order of a millisecond (see Fig. 7 for numerically computed characteristic time at the onset of wave instability). This is already on the border of the validity of the approximation of slow membrane dynamics, because such characteristic time is comparable with the time scale of conformational transitions in individual active inclusions. Therefore, our analysis of the wave instability should be viewed as only providing an indication that such an instability may exist. The accurate quantitative analysis of this instability should be performed without assuming the slowness of membrane dynamics; it will be undertaken in a separate publication. [16]

## V. DISCUSSION

We have constructed a complete kinetic description for membranes with multiple-state active inclusions. This work generalizes previous theories on active membranes [8, 9, 15]. Although we assume that all inclusions have the same orientation with respect to the membrane, the situation where inclusions with both orientations are present is a simple extension of this work. The active forcing resulting from the conformational changes of the inclusions affecting membrane dynamics through a direct force acting on the membrane (active permeation), a force dipole due to density asymmetry induced by membrane curvature, and a force quadrupole, are all present in Eq. (21). Comparing to previous theoretical works on active membranes, Eq. (21) directly connects the active forcing with each conformational

change of the inclusions.

In the limit of slow membrane dynamics, the distribution over the internal states of active inclusions adiabatically following the changes in the local membrane shape. Our theory recovers the active force dipoles and active force quadrupoles introduced in previous theories [5, 15]. Furthermore, the linearized equations of motion (40)(41) reveal that the effective elastic moduli of the membrane are renormalized both by the active forcing resulting from inclusion conformation changes and the distribution over the internal states of the inclusions. Thus, our linearized equations of motion can be applied to analyze the experimentally observed renormalization of the membrane rigidity [6] and surface tension [7] by inclusion activities. It would be interesting to see how the pumping effect due to the nonequilibrium forcing and the non-pumping effect due to the nonequilibrium inclusion distribution over the internal states contribute to the observed mechanical properties of an active membrane. [16]

We also show that when the system is driven sufficiently far away from the equilibrium state, a uniform membrane becomes unstable and, besides a long-wavelength instability arising from negative effective surface tension, static Turing-type or traveling waves spontaneously develop in the system. Figure 3 shows that the possible instabilities for an active membrane depend on the signs of the active force dipole  $p_A$ , active force quadrupole  $Q_A$ , and whether inclusion activity is sensitive to the local membrane curvature (described by the magnitude of the parameter  $l_K$ ). For inclusions whose activity is highly sensitive to the local membrane curvature, it is possible for a static Turing-type instability with a characteristic length of the order of hundreds nanometers to take place. For inclusions whose  $p_A$ ,  $Q_A$ , renormalized elastic constants  $c_{eff}^h$  and  $c_{eff}^\phi$  all having the same sign and activity is not very sensitive to the local membrane curvature, it is possible for a wave-instability to take place. The characteristic length of the traveling wave is of the order of hundreds of nanometers and characteristic frequency is of the order of a thousand Hz or less.

For traveling waves with frequency of the order of a thousand Hz, the characteristic time is already comparable with the time scale of conformational transitions in individual active inclusions. Therefore, in the accurate quantitative analysis of this type of waves, the inclusion distribution over the internal states should not adiabatically follow the changes in the local membrane shape. Such analysis should start from Eq. (21), waves with high frequency and wavelength of the order of hundreds of nanometers should manifest themselves as the synchronization of inclusion conformational cycles. [16]

We believe our theory will inspire new experiments on the active membranes. Once  $p_A$  and  $Q_A$  of the inclusions are identified through the measurements of the surface tension and the bending modulus of the passive and active membranes, the criterions for the instabilities can be deduced from our theory. The static Turing instability may be observed by optical microscope, and both stationary and traveling waves can be detected by dynamics scattering experiments. In the future, it is also possible to design “active vesicles” whose morphology and mobility are controlled by the activities of the inclusions. Such active vesicles may harvest the energy supply in the environment, turn chemical energy into mechanical energy, and act as membrane machines.

### Acknowledgement

HYC thanks stimulating discussions with J-F. Joanny and P. Bassereau. HYC is supported by National Science Council of the Republic of China (Taiwan) under grant number NSC 96-2628-M-008 -001 -MY2.

### Appendix

In this appendix we give a brief calculation that relates the shape of a conical state- $\alpha$  inclusion to its coupling constant  $c_\alpha$ .

As shown in figure 8, the outer radius, inner radius, and the thickness of a state- $\alpha$  inclusion are  $r_\alpha^{out}$ ,  $r_\alpha^{in}$ , and  $l_\alpha$ , respectively. The preferred radius of curvature  $R_\alpha$  is related to these quantities by

$$\frac{r_\alpha^{out}}{R_\alpha + l_\alpha/2} = \frac{r_\alpha^{in}}{R_\alpha - l_\alpha/2}.$$

That is,

$$R_\alpha = \frac{l_\alpha(r_\alpha^{out} + r_\alpha^{in})/2}{r_\alpha^{out} - r_\alpha^{in}} = \frac{(r_\alpha^{out} + r_\alpha^{in})^2 l_\alpha/2}{(r_\alpha^{out})^2 - (r_\alpha^{in})^2} \sim \frac{\Sigma_\alpha l_\alpha}{\Delta \Sigma_\alpha}, \quad (50)$$

where  $\Sigma_\alpha$  is the average cross-sectional area of a state- $\alpha$  inclusion,  $\Delta \Sigma_\alpha$  is the difference of cross-sectional area between the outer and inner surfaces of a state- $\alpha$  inclusion. The coupling constant  $c_\alpha$  is simply  $c_\alpha \sim 1/R_\alpha$ . From Eq. (2)(4), regions rich in  $c_\alpha > 0$  inclusions tend to have  $\nabla^2 h < 0$ , this is illustrated in Fig. 9.

- 
- [1] H. Lodish *et al.*, *Molecular cell biology*, 3rd ed. (W.H. Freeman, New York, 1995), 3rd ed.
- [2] E. Sackmann, *J. Phys.: Condens. Matter*, **18**, R785 (2006).
- [3] U. Seifert, *Adv. Phys.*, **46**, 13 (1997).
- [4] J. Prost and R. Bruinsma, *Europhys. Lett.*, **33**, 321 (1996).
- [5] J.-B. Manneville, P. Bassereau, S. Ramaswamy, and J. Prost, *Phys. Rev. E*, **64**, 021908 (2001).
- [6] P. Girard, J. Prost, and P. Bassereau, *Phys. Rev. Lett.*, **94**, 088102 (2005).
- [7] M.M. El Alaoui Faris, D. Lacoste, J. Pècrèaux, J-F. Joanny, J. Prost, and P. Bassereau, *Phys. Rev. Lett.*, **102**, 038102 (2009).
- [8] S. Ramaswamy, J. Toner, and J. Prost, *Phys. Rev. Lett.*, **84**, 3494 (2000).
- [9] H-Y. Chen, *Phys. Rev. Letts.*, **92**, 168101, (2004).
- [10] C-H. Chen and H-Y. Chen, *Phys. Rev. E*, **74**, 051917 (2006).
- [11] Needham. D. and R. M. Hochmuth, *Biophys. J.* **61**, 1664, (1992).
- [12] H. Strey, M. Peterson, and E. Sackmann, *Biophys. J.* **69**, 478, (1995).
- [13] See, for example, R.R. Netz and P. Pincus, *Phys. Rev. E*, **52**, 4114 (1995).
- [14] P. Sens and M.S. Turner, *Biophys. J.*, **86**, 2049 (2004).
- [15] M.A. Lomholt, *Phys. Rev. E* **73**, 061913 (2006).
- [16] H-Y. Chen and A.S. Mikhailov, unpublished.

TABLE I: notations in Eq. (2)(3)(4)(21)(22)

symbol	physical meaning	typical value
$\kappa$	membrane bending modulus	$\sim 10k_B T$
$\gamma$	membrane surface tension	$\lesssim 5 \times 10^{-3} k_B T / \text{nm}^2$
$c_\alpha$	inclusion-curvature coupling constant	$\lesssim 0.1 \text{nm}^{-1}$
$k_2$	higher bending modulus for the membrane	$\sim 300k_B T \cdot \text{nm}^2$
$a$	lateral linear size of an inclusion	5nm
$n_0$	$1/a^2$	$\sim 0.04 \text{nm}^{-2}$
$\eta$	solvent viscosity	$\sim 0.01 - 0.1 \text{g/cm} \cdot \text{s}$
$k_{\alpha\beta}$	inclusion conformational transition rate	$\sim \text{ms}^{-1} - \mu\text{s}^{-1}$
$P_{\alpha\beta}^m$	momentum transfer to the membrane for $\beta \rightarrow \alpha$ inclusion conformational change	$\sim \text{pN} \cdot \mu\text{s} - \text{pN} \cdot \text{ms}$
$P_{\alpha\beta}$	momentum transfer to the solvent for $\beta \rightarrow \alpha$ inclusion conformational change	$\sim \text{pN} \cdot \mu\text{s} - \text{pN} \cdot \text{ms}$
$z_{\alpha\beta}^{(u)}, z_{\alpha\beta}^{(d)}$	characteristic lengths associated with active force during $\beta \rightarrow \alpha$ transition	$\sim \text{nm}$

TABLE II: notations in Eq. (40)

symbols	definition	physical meaning
$\psi_\alpha, l_{\psi\alpha}$	$\phi_\alpha/\phi_t = \psi_\alpha(1 + l_{\psi\alpha}\nabla^2 h)$	represent the relative density of state- $\alpha$ inclusions
$\kappa_{eff}$	$\kappa(1 + \sum_\alpha \psi_\alpha l_{\psi\alpha} \phi_{t0})$	effective bending rigidity in $\delta F/\delta h$
$c_{eff}^h$	$\sum_\alpha c_\alpha \psi_\alpha \kappa / \kappa_{eff}$	inclusion-curvature coupling in $\delta F/\delta h$
$c_{eff}^\phi$	$\sum_\alpha M_\alpha (\kappa c_\alpha + n_0 k_B T l_{\phi\alpha}) / M_{eff} \kappa_{eff}$	inclusion-curvature coupling in $\partial\phi_t/\partial t$
$K_0$	$K_s = K_0(1 + l_K \nabla^2 h)$	$K_0 \phi_t$ is the curvature-independent conformational current
$l_K$	$K_s = K_0(1 + l_K \nabla^2 h)$	$K_0 l_k (\nabla^2 h) \phi_{t0}$ is the curvature-dependent conformational current
$\gamma_a$	$\gamma + n_0 p_A K_0 \phi_{t0}$	surface tension renormalized by active force dipoles
$\kappa_a$	$\kappa_{eff} - n_0 Q_A K_0 l_K \phi_{t0}$	bending rigidity renormalized by curvature-induced active quadrupoles
$c_a$	$(\kappa_{eff} c_{eff}^h - n_0 Q_A K_0) / \kappa_{eff}$	inclusions-curvature coupling renormalized by curvature-independent active force quadrupoles

TABLE III: typical magnitudes of parameters that are important for stability analysis

symbol	physical meaning	typical magnitude
$p_A$	active force dipole	$ p_A /a \lesssim \text{pN} \cdot \text{ms}$
$Q_A$	active force quadrupole	$ Q_A /a^2 \lesssim \text{pN} \cdot \text{ms}$
$K_0$	characteristic time scale for curvature-independent inclusion conformational-change cycle	$ K_0  \lesssim \text{ms}$
$K_0 l_K \nabla^2 h$	characteristic time scale of curvature-induced inclusion conformational-change cycle	$ K_0 l_K \nabla^2 h  \lesssim \text{ms}$
$\phi_{t0}$	average areal fraction of the inclusions	$\phi_{t0} \lesssim 0.1$
$\chi_{eff}$	effective susceptibility of the inclusions	$\chi_{eff} \sim k_B T / \text{nm}^2$
$\kappa_{eff}$	effective membrane curvature elastic modulus	$\kappa_{eff} \lesssim 10 k_B T$
$c_{eff}^h, c_{eff}^\phi$	effective inclusion-curvature elastic coupling constants	$ c_{eff}^h ,  c_{eff}^\phi  \lesssim 0.1 \text{nm}^{-1}$



## Figure Captions

- Figure 1. Force centers of the active force dipoles for  $\beta \rightarrow \alpha$  transitions are distributed on surfaces described by  $h + z_{\alpha\beta}^{(u)}$ , and  $h - z_{\alpha\beta}^{(d)}$ . These surfaces and  $h(\mathbf{r})$  are parallel surfaces, the areas of parallel surface elements from top to bottom are  $(1 - z_{\alpha\beta}^{(u)} \nabla^2 h) dA$ ,  $dA$ , and  $(1 + z_{\alpha\beta}^{(d)} \nabla^2 h) dA$ .
- Figure 2. Schematics of the conformational transitions of an inclusion with five internal states. When one considers the dynamics of the system at lengths large compared to  $\mathcal{O}(10 \text{ nm})$ , the strength of the conformational current of an inclusion with characteristic time scale comparable to typical ion pumps is described  $K_s \phi_t$ .
- Figure 3. Phase diagrams for membranes containing active inclusions.  $\gamma = 10^{-4} k_B T / \text{nm}^2$ ,  $k_2 = 250 k_B T \cdot \text{nm}^2$ ,  $\phi_{t0} = 0.1$ ,  $M_{eff} \chi_{eff} = 1 \mu\text{m}^2 / \text{s}$ ,  $\eta = 10^{-3} \text{kg} / \text{m} \cdot \text{s}$ . Long-dashed curve indicates the onset of wave instability, short-dashed curve indicate the onset of Turing instability, solid line indicates the onset of long wavelength instability. The phase boundaries are determined by taking  $\kappa_{eff} = 5 k_B T$  and  $c_{eff}^h = c_{eff}^\phi = 0.1 \text{nm}^{-1}$  at the onset of all instabilities. (a)  $p_A/a = 1 \text{pN} \cdot \text{ms}$ ,  $Q_A/a^2 = 1 \text{pN} \cdot \text{ms}$ . For inclusions with  $l_K/a$  greater than the slope of the dashed line, the system has Turing-type instability at large energy input, otherwise the system has wave instability. (b)  $p_A/a = 1 \text{pN} \cdot \text{ms}$ ,  $Q_A/a^2 = -1 \text{pN} \cdot \text{ms}$ . In this case, only Turing-type instability occurs at high energy input. (c)  $p_A/a = -1 \text{pN} \cdot \text{ms}$ ,  $Q_A/a^2 = 1 \text{pN} \cdot \text{ms}$ . For inclusions with  $l_K/a$  greater than the slope of the dashed line, the system has Turing-type instability at large energy input, otherwise the system has long wavelength instability. (d)  $p_A/a = -1 \text{pN} \cdot \text{ms}$ ,  $Q_A/a^2 = -1 \text{pN} \cdot \text{ms}$ . For inclusions with  $|l_K/a|$  greater than the absolute value of the slope of the dashed line, the system has Turing-type instability at large energy input, otherwise the system has long wavelength instability.
- Figure 4. Mechanism for Turing-type instability: (i) inclusions are attracted to regions with preferred curvature, (ii) curvature-dependent active force quadrupoles generate membrane curvature that inclusions prefer. This positive feedback leads to a Turing-type instability.
- Figure 5. characteristic wavelengths at the onset of instabilities for  $\gamma = 10^{-4} k_B T / \text{nm}^2$ ,

$k_2 = 250k_B T \cdot \text{nm}^2$ ,  $\phi_{t0} = 0.1$ ,  $M_{eff}\chi_{eff} = 1\mu\text{m}^2/\text{s}$ ,  $\eta = 10^{-3}\text{kg}/\text{m} \cdot \text{s}$ .  $\kappa_{eff} = 5k_B T$ , and  $c_{eff}^h = c_{eff}^\phi = 0.1\text{nm}^{-1}$ . The characteristic wavelengths are on the order of 100nm for all cases except at the vicinity of long-wavelength instabilities, where the characteristic lengths increase abruptly. (a) thin curves:  $p_A/a = 1\text{pN} \cdot \text{ms}$ ,  $Q_A/a^2 = 1\text{pN} \cdot \text{ms}$  (dashed curve: wave instability, solid curve: Turing-type instability); thick curves:  $p_A/a = 0.1\text{pN} \cdot \text{ms}$ ,  $Q_A/a^2 = 1\text{pN} \cdot \text{ms}$  (dashed curve: wave instability, solid curve: Turing-type instability). (b) dashed curve:  $p_A/a = -1\text{pN} \cdot \text{ms}$ ,  $Q_A/a^2 = 1\text{pN} \cdot \text{ms}$ ; and solid curve:  $p_A/a = -1\text{pN} \cdot \text{ms}$ ,  $Q_A/a^2 = -1\text{pN} \cdot \text{ms}$ .

- Figure 6. Mechanism for wave instability: (i) inclusions are attracted to regions with their preferred curvature (ii) in inclusion-rich domains, active force quadrupoles produce membrane curvature that inclusions dislike, the inclusions leave inclusion-rich domains and the membrane configuration goes back to (i).
- Figure 7. Characteristic time scale at the onset of wave instability for  $\gamma = 10^{-4}k_B T/\text{nm}^2$ ,  $k_2 = 250k_B T \cdot \text{nm}^2$ ,  $\phi_{t0} = 0.1$ ,  $M_{eff}\chi_{eff} = 1\mu\text{m}^2/\text{s}$ ,  $\eta = 10^{-3}\text{kg}/\text{m} \cdot \text{s}$ .  $\kappa_{eff} = 5k_B T$ , and  $c_{eff}^h = c_{eff}^\phi = 0.1\text{nm}^{-1}$ . Dashed curve:  $p_A/a = 1\text{pN} \cdot \text{ms}$ ,  $Q_A/a^2 = 1\text{pN} \cdot \text{ms}$ ; solid curve:  $p_A/a = 0.1\text{pN} \cdot \text{ms}$ ,  $Q_A/a^2 = 1\text{pN} \cdot \text{ms}$ . The magnitude of  $l_K/a$  for the solid curve is indicated at the top of the frame, and the magnitude of  $l_K/a$  for the dashed curve is indicated at the bottom.
- Figure 8. A conical inclusion in state  $\alpha$ ,  $l_\alpha$  is the thickness of the inclusion,  $r_\alpha^{out}$  is the outer radius,  $r_\alpha^{in}$  is the inner radius of the inclusion.
- Figure 9. Regions rich in positive  $c_\alpha$  inclusions tend to have  $\nabla^2 h < 0$ .

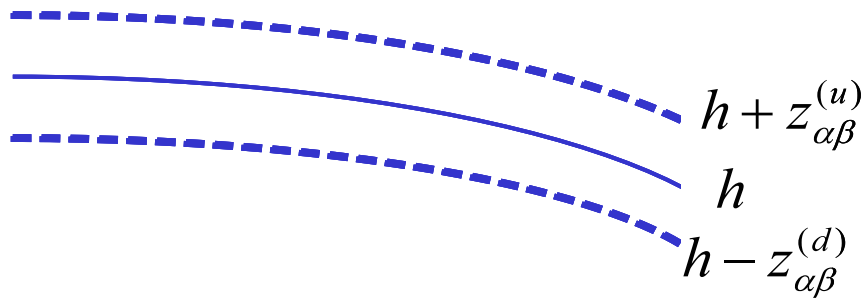


FIG. 1:

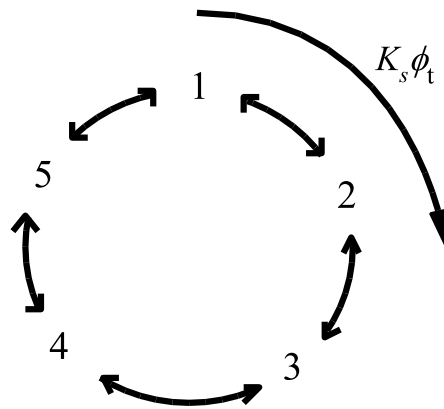
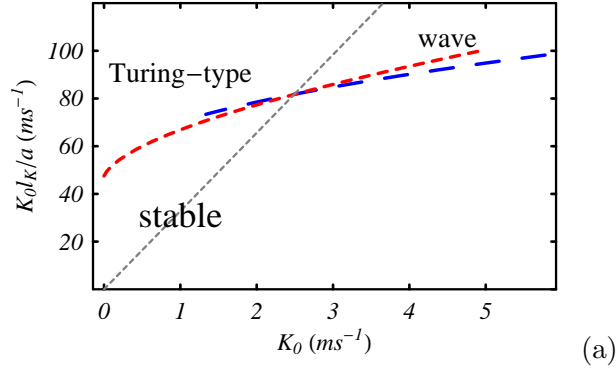
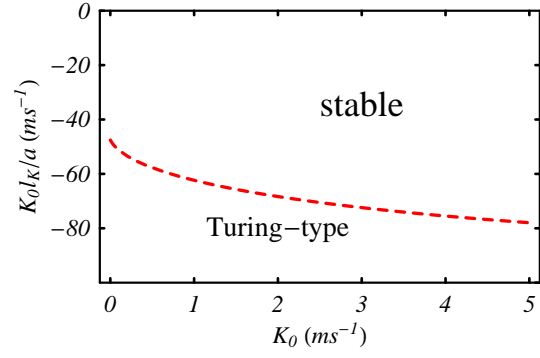


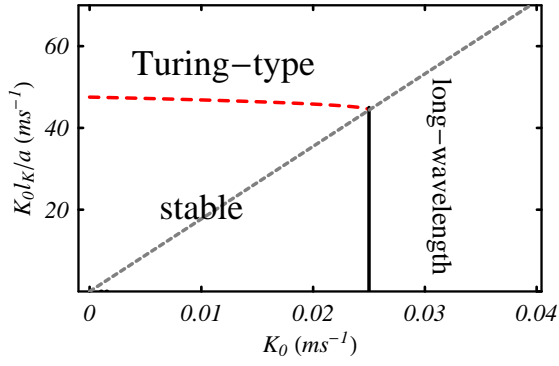
FIG. 2:



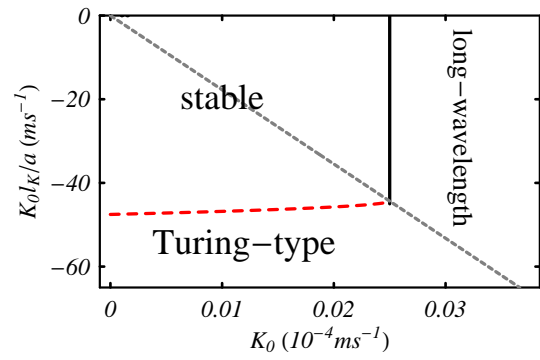
(a)



(b)



(c)



(d)

FIG. 3:

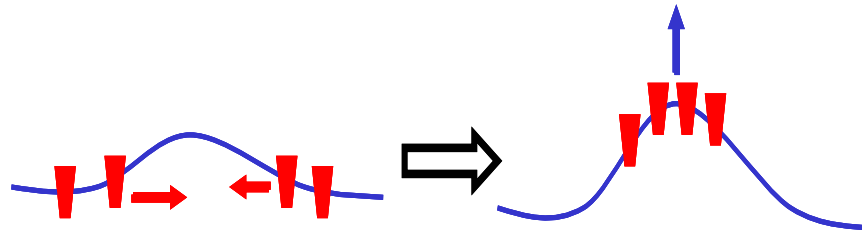
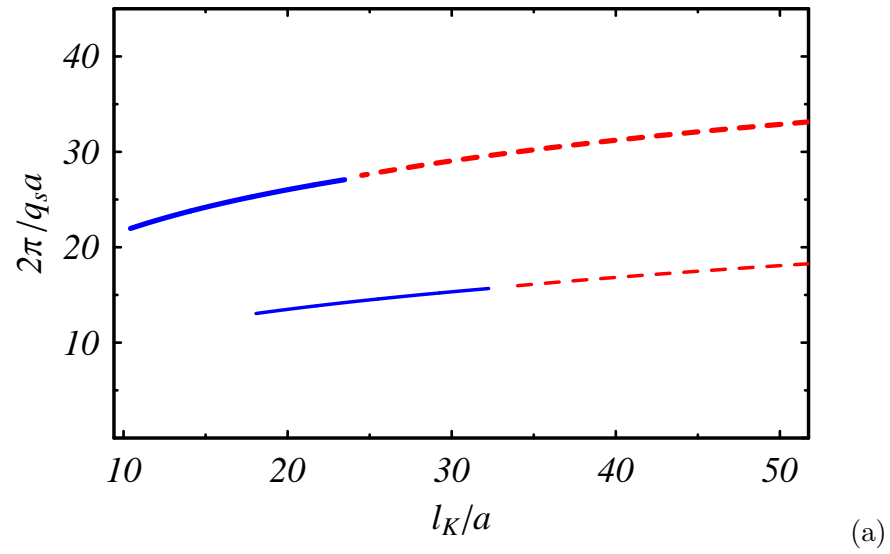
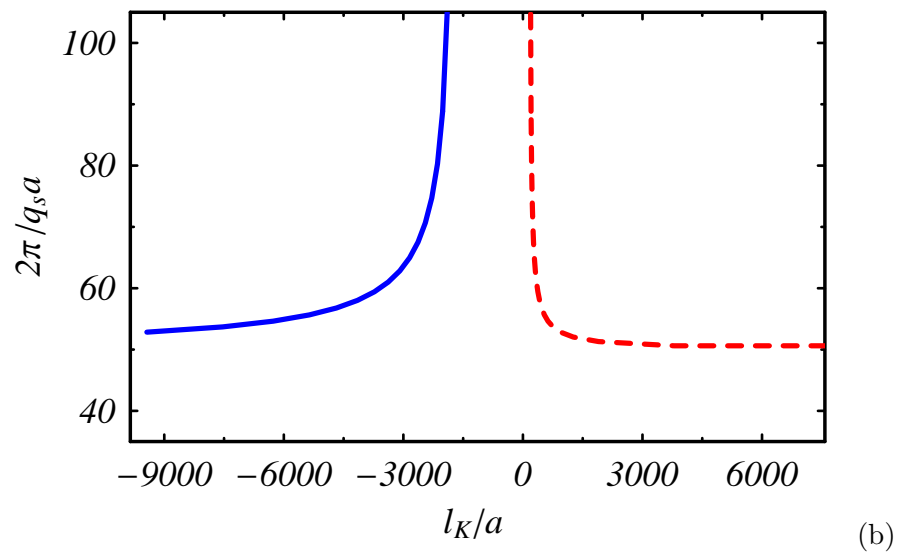


FIG. 4:



(a)



(b)

FIG. 5:

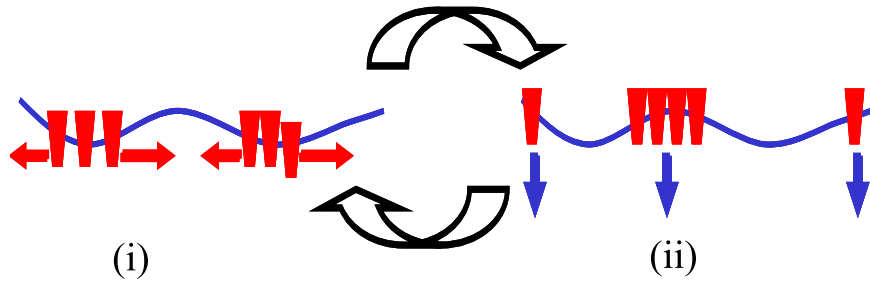


FIG. 6:

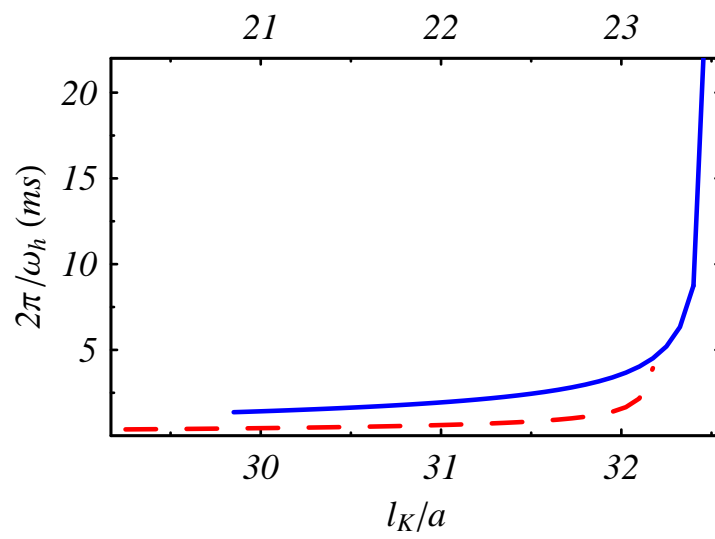


FIG. 7:

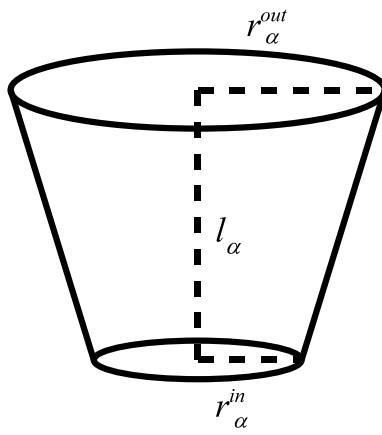


FIG. 8:

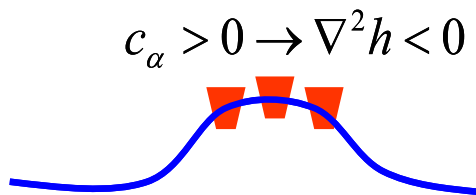


FIG. 9: